$\gamma_0$ in Eq. (6) and has been drawn in Fig. 2 for comparison with actual data.

For the (400) reflection, four measurements of $(f+\Delta f')^2+(\Delta f'')^2$ were made with the thinnest crystal and two with the crystal of intermediate thickness (44 $\mu$). These results are averaged to give the value listed in Table II. The measured atomic scattering factor listed for the (511) and the (333) reflections result from an averaging of ten measurements each on the thin crystal.

It is interesting to note the similiarity between the measured form factors of nickel and aluminum.[12] For both fcc metals, the form factor for the first two reflections are lower than theory with the scattering factor of the (200) reflection having the largest discrepancy. In both cases, the scattering factor of the (511) and (333) reflections indicate that the core charge distribution is spherically symmetric. Combining this with the observation that the (400) form factor of nickel is also low, leads one to suspect the possibility that the outer electrons are spread out along directions that have the smallest atomic density. It would therefore be interesting to perform measurements of atomic scattering factors in metals with different crystal symmetry and to compare the results with theoretical data obtained from accurate band calculations.

## ACKNOWLEDGMENTS

We extend our sincere appreciation and thanks to Professor A. Paoletti for his encouragement and active support throughout this joint research effort. We are also indebted to Dr. D. R. Chipman, Dr. L. D. Jennings, and Dr. W. C. Phillips for their suggestions and critical review of this work.

PHYSICAL REVIEW VOLUME 187, NUMBER 3 15 NOVEMBER 1969

# Helicon-Acoustic Dispersion Relations in Metals: Effective-Mass and Relaxation-Time Dependence*†

G. PERSKY‡ AND T. KJELDAAS, JR.
*Department of Physics Polytechnic Institute of Brooklyn, Brooklyn, New York 11201*
(Received 19 May 1969)

The electromagnetic, constitutive, and lattice equations governing propagation of transverse acoustic and electromagnetic waves in a metal with conduction electrons possessing a constant scalar effective mass, and in which there is a uniform magnetic field applied along the propagation direction, are given. These equations are used to derive a secular equation describing the dispersion of interacting helicon and acoustic waves, and in which additional structure arising from the difference between the free-electron mass and the effective electron mass is evident. Magnetoacoustic attenuation, the dispersion and damping of uncoupled helicon waves, and the helicon-acoustic interaction are then analyzed in turn. Numerical solutions of the helicon dispersion relation are presented. The dispersion curve displays a branching in the absorption-edge region. A simple analytic treatment of the relaxation-time and effective-mass dependence of the helicon-acoustic interaction is given. The interaction near and in the absorption-edge region is investigated numerically. A rather large effect of this interaction on the magnetoacoustic absorption of potassium in the edge region is found.

## I. INTRODUCTION

In recent years, the interaction of acoustic waves in metals and semiconductors with the particular magnetoplasma modes known as helicons has been of interest. Interaction between transverse ultrasound and helicons has been observed in potassium by Grimes and Buchsbaum[1] and Libchaber and Grimes.[2] Shilz[3] has studied the interaction of helicons with both longitudinal and transverse ultrasound in lead telluride. Noteworthy theoretical treatments based on the free-electron model have been given by Langenberg and Bok[4] and Quinn and Rodriquez.[5,6]

The motivating interest behind the present investigation was to arrive at a convincing description of the role of band-structure effects in the magnetoacoustic interaction in metals. A general theory of the dynamics and transport properties of localized Bloch electrons subjected to perturbations with a wavelike character has

* Work supported by Grant No. AF-AFOSR 62–258 and Contract No. AF 49-(638)-1372 from the U. S. Air Force Office of Scientific Research.

† Based on a dissertation submitted to the Polytechnic Institute of Brooklyn, in partial fulfillment of the requirements for the degree of Doctor of Philosophy (Physics), 1968.

‡ Present address: Bell Telephone Laboratories, Murray Hill, N. J.

[1] C. C. Grimes and S. J. Buchsbaum, Phys. Rev. Letters **12**, 357 (1964).

[2] A. Libchaber and C. C. Grimes, Phys. Rev. **178**, 1145 (1969).

[3] W. Shilz, Phys. Rev. Letters **20**, 104 (1968).

[4] D. N. Langenberg and J. Bok, Phys. Rev. Letters **11**, 549 (1963).

[5] J. J. Quinn and S. Rodriguez, Phys. Rev. Letters **11**, 552 (1963).

[6] J. J. Quinn and S. Rodriguez, Phys. Rev. **133**, A1589 (1964).

been developed to this end.[7] The details will be presented in two forthcoming papers. Certain of the results, specific to acoustic attenuation and the helicon-acoustic interaction are given here.

In this paper, we depart from the free-electron model, explicitly taking into account the electronic effective mass. The role of collisions is handled in the customary way through the assumption of a relaxation time. Starting from the macroscopic equations of motion of the electromagnetic fields, electronic system, and lattice, we develop, in Sec. II, the basic secular equation which describes the propagation and attenuation characteristics of an interacting helicon and transverse acoustic wave. In Sec. III we utilize this equation to derive the effective-mass dependence of the attenuation of transverse ultrasound under a variety of conditions. In Sec. IV we examine the independent helicon mode and confirm that the onset of temporal damping occurs at the expected onset for DSCR (Doppler-shifted cyclotron resonance),[8,9] while the absorption edge for spatial damping[10] occurs at a field approximately 2% (0.0195) higher. It is shown explicitly that this point separates the normal (spatially damped) helicon branch from another "backward-wave branch." The helicon-acoustic interaction is treated analytically for higher magnetic fields in Sec. V, with particular attention paid to the effective-mass dependence of the propagation and attenuation characteristics of the eigenmodes in the "crossover region." With relatively low magnetic fields, crossover can occur in the vicinity of the absorption edge of the helicon and acoustic waves. In Sec. VI numerical techniques are employed to study this regime. Calculated dispersion and absorption curves are presented for interaction between the helicon and fast transverse wave in potassium. A rather large effect of this interaction on the magnetoacoustic absorption in the edge region is demonstrated.

## II. MACROSCOPIC EQUATIONS

The convenient starting point in a treatment of the helicon-acoustic interaction is the macroscopic equations of motion of the electromagnetic field, electron system, and lattice. We shall confine our attention to the case of a monovalent metal with cubic symmetry in which there is a transverse wave with acoustic and/or electromagnetic components propagating along a fourfold axis. We shall further suppose that there is a uniform magnetic field applied parallel to the same axis. Assuming, then, a space-time dependence $e^{i(\mathbf{q}\cdot\mathbf{r}-\omega t)}$ for the wave, Maxwell's curl equations can be written

$$i\mathbf{q}\times\mathbf{E}=i(\omega/c)\mathbf{B}, \tag{1}$$

$$i\mathbf{q}\times\mathbf{B}=-i(\omega/c)\mathbf{E}+(4\pi/c)\mathbf{j}_t. \tag{2}$$

Here $\mathbf{E}$ is the electric field vector, $\mathbf{B}$ the magnetic field, and $\mathbf{j}_t$ the net current (electronic+ionic). We have taken the permeability to be that of free space, which is permissible for nonferromagnetic metals. Elimination of $\mathbf{B}$ between (1) and (2) yields

$$(q^2-\omega^2/c^2)\mathbf{E}=(4\pi i/c^2)\mathbf{j}_t. \tag{3}$$

It is evident from (3) that the displacement current can be neglected if the phase velocity of the waves of interest is very much smaller than $c$. This is always true for acoustic waves, and must also be the case for helicon waves in any regime in which helicon-acoustic interaction is possible. Consequently, we shall delete the displacement-current term when employing (3).

The remaining macroscopic equations are those of the lattice and electronic system. Both require prior solution of the Boltzmann equation for the electron distribution function. The current integral of the distribution function provides the constitutive equation relating the electron current to the fields and ion current. The time rate of change of the momentum density yields the macroscopic electron-lattice forces, which together with the macroscopic fields gives rise to perturbation terms of the equation of motion of the lattice. We have found[7] that for the parabolic band model the lattice and constitutive equations, respectively, take the form

$$\left\{q^2\left[c_{s0}^2+\frac{1}{5}\frac{m}{M}(\beta-\gamma-1)v^2\right]-\omega^2\left[1+\frac{m}{M}(1-\beta)\right]\right\}J^{\pm}$$
$$\mp\frac{eB_0}{Mc}\omega[J^{\pm}+(1-\beta)j^{\pm}]+i\frac{ne^2}{M}\beta E^{\pm}$$
$$-i\frac{m}{M}\frac{\omega}{\tau}(j^{\pm}+J^{\pm})=0, \tag{4}$$

$$j^{\pm}=\sigma_0 G^{\pm}E^{\pm}-\{(1-\beta+\gamma)$$
$$+[(\beta-\gamma)\mp i\omega_c{}^*\tau(1-\beta+\gamma)+i\omega\tau\gamma]G^{\pm}\}J^{\pm}, \tag{5}$$

where, for propagating in the $z$ direction, $J^{\pm}=J_x\pm iJ_y$, etc.; the longitudinal magnetic field leads to circularly polarized waves. In these equations $j$ is the electric current due to electrons, $J$ that due to the positively charged ions, $m$ and $m^*$ the electronic free and effective mass, respectively, $M$ the ion mass, $n$ the number of electrons (or ions) per unit volume, $v$ the Fermi velocity, $\tau$ the relaxation time at the Fermi surface, $B_0$ the $z$ component of the applied magnetic field, $c_{s0}$ the "bare lattice" sound velocity (which is due to the microscopic Coulomb and non-Coulomb interionic forces), and $\sigma_0=ne^2\tau/m^*$ the dc conductivity. The symbol $e$ stands for the actual electronic charge and is, therefore, a

[7] G. Persky, Ph.D. Dissertation, Polytechnic Institute of Brooklyn, 1968 (unpublished).
[8] T. Kjeldaas, Jr., Phys. Rev. **113**, 1473 (1959).
[9] E. A. Stern, Phys. Rev. Letters **10**, 91 (1963); M. T. Taylor, J. R. Merrill, and R. Bowers, *ibid.* **6**, 159 (1963).
[10] T. Kjeldaas, Jr., Bull. Am. Phys. Soc. **8**, 428 (1963); **8**, 446 (1963); also unpublished reports.

negative number. Thus, the cyclotron frequency $\omega_c^*=eB_0/m^*c$ is negative for $B$ in the $+z$ direction. $G^{\pm}$ is a wave vector and frequency-dependent conductivity function given by[7,8]

$$G^{\pm}=\frac{3}{4iqv\tau}\left\{\left[1+\left(\frac{1}{qv\tau}+\frac{i(\pm\omega_c^*-\omega)}{qv}\right)^2\right]\times\ln\left[\frac{\pm\omega_c^*-\omega+qv-i/\tau}{\pm\omega_c^*-\omega-qv-i/\tau}\right]+2\left(\frac{\pm\omega_c^*-\omega}{qv}-\frac{i}{qv\tau}\right)\right\}. \quad (6)$$

The parameters $\beta$ and $\gamma$ constitute the generalization of the free-electron-model equations to a model with a parabolic band, and embody the additional structure. $\beta=m/m^*$ is the ratio of the electronic free to effective mass, while $\gamma$ originates in a velocity-dependent deformation potential and is sensitive to the manner in which the self-consistent microscopic potential of the electron-ion assembly is altered by the lattice strain.[7] (There is no scalar deformation potential associated with shear waves in a cubic Bravais lattice, but components of the electron energy involving both the strain tensor and even powers of the electron energy involving both the strain tensor and even powers of the electron wave vector are not ruled out by symmetry. $\gamma$ is associated with the component of second order in the electron wave vector.) Recovery of the free-electron-model equations from (4) and (5) is accomplished by setting $m^*=m$, $\beta=1$, and $\gamma=0$.

The contributions in the second line of (4) are responsible for the acoustic attenuation and coupling to the helicon wave, as well as for changes in the sound velocity. The dominant term is that containing the electric field, and here it should be observed that the net field force on the ions is altered by the factor $\beta$. This modification occurs as a consequence of the back reaction on the lattice of the field force on the electrons. A similar effect is observed in the term involving the applied magnetic field in that the electron current is present with a factor $(1-\beta)$. If the electron current were to balance the ion current, the net result would appear simply as a multiplication by $\beta$ of the Lorentz force on the ions. The last contribution to (4) is due to the "collision drag force"[11] on the ions, which is the negative of the collision-induced time rate of change of the electronic momentum density. It does not involve the effective mass.

Examination of the terms within the curly brackets in (4) discloses that $\beta$ and $\gamma$ produce a renormalization of the bare lattice sound velocity. This is a consequence of the back reaction on the lattice of the electron acceleration components directly owing to the motion of the lattice itself. During passage through a lattice supporting a strain wave, an electron at the Fermi surface suffers perturbations in its motion as a result of the acceleration of the lattice, the inhomogeneities in the strain field, and the combination of the two. The last mentioned makes a vanishing contribution to the force density when averaged over the Fermi surface. The first mentioned may be identified with the "induced velocity" discussed by Holstein,[11] and is always experienced by a Bloch electron when the host lattice is in nonuniform motion. It gives rise to the renormalization coefficient multiplying $\omega^2$, which is exceedingly small and may be neglected. The strain inhomogeneities result in an electron acceleration proportional to $(\mathbf{q}\cdot\mathbf{v})^2$, and with a magnitude that is also dependent on the deformation parameter $\gamma$, as well as the effective mass. Consequently, $\gamma$ appears in the associated renormalization coefficient. The factor $\frac{1}{5}$ is a result of averaging over the Fermi surface. It is not difficult to see that this renormalization could, in principle, be appreciable. We have made numerical estimates[7] of $\gamma$ for the alkali metals and have found it to be sufficiently small to justify setting $\gamma=0$ in (4) and (5) unless one specifically wants to study its effects. Upon performing this step and absorbing $(\beta-1)mv^2/5M$ into a renormalized sound velocity $c_s=[c_{s0}^2+(\beta-1)mv^2/5M]^{1/2}$, (4) and (5) become

$$(q^2-\omega^2)J^{\pm}+\rho\left\{\mp\frac{\omega_c^*\omega}{\beta}[J^{\pm}+(1-\beta)j^{\pm}]+i\frac{ne^2}{m}\beta E^{\pm}-i\frac{\omega}{\tau}(j^{\pm}+J^{\pm})\right\}=0, \quad (7)$$

$$j^{\pm}=\sigma_0 G^{\pm}E^{\pm}-\{(1-\beta)+[\beta\mp i\omega_c^*\tau(1-\beta)]G^{\pm}\}J^{\pm}, \quad (8)$$

where $\rho\equiv m/M$.

Inspection of the constitutive equation in its simplified form (8) now discloses the following properties: (a) the functional dependence of the electron current on the electric field is of the same form as for the free-electron model, (b) there is an "induced velocity" contribution $(1-\beta)J$, (c) the collision drag term appears with a coefficient $\beta$; in combination with the induced velocity term this yields a value of $j=-J$ for $E=\tau=0$, and (d) there is a cyclotron-frequency-dependent contribution that has no counterpart in the free-electron model. In part, it arises from the perturbations of electronic motion already discussed in connection with (4), but also includes components attributable to variations in the Lorentz force acceleration resulting from strain-induced changes in the effective mass.[7]

Equations (3), (7), and (8) constitute the required set of homogeneous simultaneous equations for the three unknowns $j$, $J$, and $E$ [$j_t=j+J$ in (3)]. Setting the determinant of their coefficients to zero will yield a secular equation from which the dispersion relations of the eigenmodes can be obtained. However, the form of this equation is not particularly transparent. It would be preferable to have a secular equation in which the coupling of the helicon and acoustic waves is manifest.

[11] T. Holstein, Phys. Rev. **113**, 479 (1959).

The latter can easily be obtained through (a) replacement of $j$ by the net current $j_t$, as an independent variable in (7) and (8), and (b) elimination of the constitutive equation. The reasoning is as follows. For a pure helicon mode there is no ion current. On the other hand, for transverse acoustic waves in metals at frequencies up to the kilomegacycle range there is quasibalance of currents,[12] which means that the self-consistent electric field produced is just that necessary to make the electron current equal and opposite to the ion current. Hence, the acoustic-dispersion relation in the quasi-current-balance regime may be extracted from the constitutive and lattice equations with the net current set equal to zero; the electromagnetic equation does not play a role. Therefore, the procedure described above must lead to a secular equation composed of the product of the independent helicon and acoustic dispersion relations and an additive interaction term. Following this program, we set $j=j_t-J$ in (7) and (8), which yields

$$(q^2-\omega^2\mp\rho\omega\omega_c^*)J^\pm + \rho\left[\mp\frac{\omega_c^*\omega}{\beta}(1-\beta)-i\frac{\omega}{\tau}\right]j_t^\pm+i\frac{ne^2}{m}\beta E^\pm=0, \quad (9)$$

$$j_t^\pm=\sigma_0 G^\pm E^\pm+\{\beta-[\beta\mp i\omega_c^*\tau(1-\beta)]G^\pm\}J^\pm. \quad (10)$$

We now use the constitutive equation (10) to eliminate the electric field in (3) and (9). This results in the pair of equations

$$[q^2-i\beta(\omega_p/c)^2\omega\tau G^\pm]j_t^\pm -[\beta(1-G^\pm)\pm i\omega_c^*\tau(1-\beta)G^\pm]q^2J^\pm=0, \quad (11)$$

$$\left[q^2-\frac{\omega^2}{c_s^2}\mp\rho\frac{\omega\omega_c^*}{c_s^2}\beta+\frac{i\rho\omega}{c_s^2\tau}\beta\left(1-\frac{1}{G^\pm}\right)\right]J^\pm + \frac{\rho}{c_s^2}\left[\omega_c^*\omega\left(1-\frac{1}{\beta}\right)-i\frac{\omega}{\tau}\left(1-\frac{1}{G^\pm}\right)\right]j_t^\pm=0, \quad (12)$$

where $\omega_p^2=4\pi ne^2/m$ and the first and second of which, respectively, contain the helicon and acoustic dispersion relations. By equating to zero the determinant of the coefficients of (11) and (12), we obtain the secular equation

$$\left[q^2-i\beta\left(\frac{\omega_p}{c}\right)^2\omega\tau G^\pm\right]\left[q^2-\frac{\omega^2}{c_s^2}\mp\rho\frac{\omega\omega_c^*}{c_s^2}\beta+\frac{i\rho\omega}{c_s^2\tau}\beta\left(1-\frac{1}{G^\pm}\right)\right] +(\rho/c_s^2)[\beta(1-G^\pm)\pm i\omega_c^*\tau(1-\beta)G^\pm] \times\left[\omega_c^*\omega\left(1-\frac{1}{\beta}\right)-i\frac{\omega}{\tau}\left(1-\frac{1}{G^\pm}\right)\right]=0, \quad (13)$$

that will provide the basis for the analysis in the remainder of this paper. The first line is the product of the dispersion relations of the pure helicon wave (for the proper case of $G$) and the acoustic wave in the regime of quasibalance of currents. The second line represents the helicon-acoustic coupling. The amount of additional structure present in (13), particularly in the coupling term, because of the effective mass is made most evident by comparison with its counterpart for the free-electron model. The latter is obtained from (13) simply by setting $m^*=m$, and is seen to be

$$\left[q^2-i\left(\frac{\omega_p}{c}\right)^2\omega\tau G^\pm\right]\left[q^2-\frac{\omega^2}{c_s^2}\mp\rho\frac{\omega_c\omega}{c_s^2}+\frac{i\rho\omega}{c_s^2\tau}\left(1-\frac{1}{G^\pm}\right)\right] +\frac{i\rho\omega}{c_s^2\tau}\frac{(1-G^\pm)^2}{G^\pm}q^2=0. \quad (14)$$

We shall show that the greater complexity of (13) has only minor consequences for the helicon-acoustic interaction, although the (absolute) acoustic attenuation is highly effective-mass-dependent.

## III. ACOUSTIC DISPERSION RELATIONS

The dispersion relation for the pure acoustic mode under the condition of quasibalance of currents is recovered from (13) by equating to zero the second factor in the first line, i.e.,

$$q^2=\frac{\omega^2}{c_s^2}\pm\rho\frac{\omega\omega_c^*}{c_s^2}\beta-\frac{i\rho\omega}{c_s^2\tau}\beta\left(1-\frac{1}{G^\pm}\right). \quad (15)$$

Clearly, the last two terms on the right-hand side of (15) must be responsible for any attenuation and dispersion that may be present. Since both these terms contain the electron-to-ion-mass ratio $\rho$, it is reasonable to expect the departures from the zero-order wave vector to be small. Thus, if we let $q=q_0+\delta q$, where $q_0=\omega/c_s$ is the zero-order wave vector, then $\delta q\ll q_0$ and to first order (15) becomes

$$\delta q^\pm=(\rho\beta/2c_s)[\pm\omega_c^*-(i/\tau)(1-1/G^\pm)]. \quad (16)$$

In (16), $q_0$ may be used as the wave-vector argument of $G^\pm$. The amplitude attenuation $\alpha$ is given by the imaginary part of (16), while the variation in phase velocity, $\delta c_\varphi$, is related to the real part

$$\alpha^\pm=(\rho\beta/2c_s\tau)\,\mathrm{Re}(1/G^\pm-1), \quad (17)$$

$$\delta c_\varphi{}^\pm=-(\rho\beta c_s/2\omega)[\pm\omega_c^*-\mathrm{Im}(1/\tau G^\pm)]. \quad (18)$$

These equations differ from their free-electron-model counterparts by the presence of the factor $\beta$ and the implicit dependence of $G^\pm$ on $m^*$. For the field-free case, (17) agrees with Blount's expression[13] for the quasi-current-balance transverse attenuation if one takes his constant $|A|^2$ as equal to unity.

[12] A. B. Pippard, Phil. Mag. **2**, 1147 (1957).

[13] E. I. Blount, Phys. Rev. **114**, 418 (1959).

The most outstanding feature of the transverse attenuation, when there is a longitudinal magnetic field, is the existence of an absorption edge resulting from DSCR.[8] The position of this edge and the shape of the attenuation curve is not dependent on the effective mass (for a spherical band). Our present concern is, therefore, only with the absolute magnetoacoustic attenuation, which is effective-mass-dependent. We first consider the collisionless limit $\tau\to\infty$. Then, upon neglecting $\omega$ in comparison with $\omega_c^*$ and $q_0v$, the conductivity function (6) reduces to

$$G^{\pm}=\frac{3m^*}{4iq_0\tau\hbar k_F}\left[(1-\Gamma_0^2)\ln\left(\frac{\pm\Gamma_0+1}{\pm\Gamma_0-1}\right)\pm 2\Gamma_0\right], \quad (19)$$

where

$$\Gamma_0\equiv\omega_c^*/q_0v=eB_0/\hbar ck_Fq_0, \quad (20)$$

and $k_F(=m^*v/\hbar)$ is the wave vector at the Fermi surface. Since $k_F$, and hence $\Gamma_0$, is independent of $m^*$ the only effective-mass dependence in (19) is that which is explicit in the numerator. Substitution of (19) into (17) and (18) yields

$$\alpha^{\pm}=-\frac{2}{3}\frac{\rho\beta^2q_0\hbar k_F}{mc_s}\times\mathrm{Im}\left[(1-\Gamma_0^2)\ln\left(\frac{\pm\Gamma_0+1}{\pm\Gamma_0-1}\right)\pm 2\Gamma_0\right]^{-1}, \quad (21)$$

$$\delta c_{\varphi}=\frac{\rho\beta^2\hbar k_F}{m}\times\left\{\frac{2}{3}\mathrm{Re}\left[(1-\Gamma_0^2)\ln\left(\frac{\pm\Gamma_0+1}{\pm\Gamma_0-1}\right)\pm 2\Gamma_0\right]^{-1}\mp\tfrac{1}{2}\Gamma_0\right\}. \quad (22)$$

Therefore, both the absolute magnetoacoustic attenuation (which is present only for $\Gamma_0<1$, i.e., inside the edge) and sound velocity variation are inversely proportional to the square of the effective mass; this relationship remains valid when the field is reduced to zero.

The zero-field limit of the attenuation has a different effective-mass dependence when the relaxation time is very small. For $B_0=0$ and $q_0v\tau\ll 1$, Eq. (6) can be expanded as

$$G=1-\tfrac{1}{5}(q_0v\tau)^2+(3/35)(q_0v\tau)^4+\cdots, \quad (23)$$

where we have dropped the superscripts on $G$, as they are not relevant to the zero-field case. The leading term in the resultant attenuation expression is

$$\alpha=\frac{\rho\beta}{10c_s\tau}(q_0v\tau)^2=\frac{\rho\omega^2\tau\hbar^2k_F^2}{10c_s^2m^2}\beta^3, \quad (24)$$

which displays an inverse cubic dependence on the effective mass. In this regime, the variation with frequency of the sound velocity is negligible.

We have also derived expressions for the field-free attenuation and velocity variation without the current balance assumption. As frequencies and wavelengths for which the underlying semiclassical dynamics may still be considered valid, the results do not depart significantly from those presented here. When a longitudinal magnetic field is present, the lack of current balance at reasonable frequencies is closely related to the helicon-acoustic interaction, and is best examined in that context.

## IV. HELICON DISPERSION RELATIONS

When the constraint $J=0$ is applied to the ion-electron assembly, the remaining dispersion relations (for $\mathbf{q}\|z$) are given by the first factor in the first line of (13). These correspond to + and − circularly polarized magnetoplasma modes, one of which, termed the helicon wave,[14] can propagate in the bulk. The other has an essentially imaginary wave vector and cannot transport energy. If $\mathbf{B}_0$ is oriented in the $-z$ direction, so that $\omega_c^*$ is positive for electrons, the + mode is the propagating helicon and has the dispersion relation

$$q^2-i\beta(\omega_p/c)^2\omega\tau G^+=0. \quad (25)$$

In general, (25) is a transcendental equation, but limiting cases can be treated algebraically.

### A. High-Field Limit: $(qv/\omega_c^*)\to 0$; $\omega_c^*\tau\gg 1$

In this regime, $G^+$ is well approximated by

$$G^+=(1+i\omega_c^*\tau)^{-1}, \quad (26)$$

and results in the well-known helicon dispersion relation[14]

$$q^2=\beta(\omega/\omega_c^*)(\omega_p/c)^2(1+i/\omega_c^*\tau), \quad (27)$$

for a local conductivity. Equation (27) can be re-expressed as

$$q^2=(4\pi ne/B_0c)\omega(1+i/\omega_c^*\tau), \quad (28)$$

showing explicitly that the dispersion is independent of the effective mass (or the free mass), which, however, does enter into the attenuation

$$\alpha\approx\left(\frac{4\pi ne\omega}{B_0c}\right)^{1/2}\Big/2\omega_c^*\tau=\frac{m^*}{\tau}\left(\frac{\pi n\omega c}{eB_0^3}\right)^{1/2}. \quad (29)$$

### B. Collisionless Limit with Moderately High Field: $\omega_c^*\tau\to\infty$; $(qv/\omega_c^*)\ll 1$

Here we neglect the dissipation, but take into account the nonlocality of the conductivity that becomes manifest when $qv/\omega_c^*$ is not entirely negligible. Expan-

[14] P. Aigrain, in *Proceedings of the International Conference on Semiconductor Physics, Prague, 1960* (Academic Press Inc., New York, 1961), p. 224; R. Bowers, C. Legendy, and F. Rose, Phys. Rev. Letters 7, 339 (1961).

sion of (19) in inverse powers of $\Gamma_0$ yields

$$G^+\approx(i\omega_c^*\tau)^{-1}(1+1/5\Gamma_0^2+\cdots), \tag{30}$$

leading to the dispersion relation

$$\omega=\frac{B_0c}{4\pi ne}q^2\left[1+\frac{1}{5}\left(\frac{\hbar ck_Fq}{eB_0}\right)^2+\cdots\right]^{-1}. \tag{31}$$

Therefore, when the electrons can significantly change their phase front position during a cyclotron period, the relation of $\omega$ to $q$ falls below the quadratic dependence of the high-field limit.

In order to treat the more interesting regime of high spatial dispersion in the vicinity of the absorption edge,[8,9] as well as arbitrary relaxation time, it is necessary to resort to numerical solutions of (25); at the absorption edge, $G^+$ has a singularity which makes it difficult to find useful series expansions in that region. Utilizing the full conductivity expression (6), we have calculated the helicon dispersion and absorption for potassium. The Fermi wave vector was taken as $7.47\times10^7$ cm$^{-1}$ and $\omega_p^2$ as $0.451\times10^{32}$ sec$^{-2}$, appropriate to a lattice constant of 5.2 Å. Figure 1(a) shows the dispersion curve $\omega$ versus $q_r\equiv\mathrm{Re}(q)$ computed for an infinite relaxation time and a field strength of 57.9 kG. The most significant feature of this curve is that it branches in the absorption-edge region. The branch point, which occurs at $\Gamma\equiv(\omega_c^*-\omega/q_rv)\approx1.02$, is the absorption edge for *spatial* damping of the left branch.[10] This has been observed experimentally.[2] On the other hand, the precise location of the DSCR edge is at $\Gamma=1$. It has been shown[6,10] that the onset of *temporal* damping of the right-hand branch coincides with this edge. That the dispersion curve actually branches appears to have been generally overlooked, although the occurrence of an anomaly in the surface impedance associated with the point $\Gamma\approx1.02$ has been known for some time.[15,16] This has been attributed to the zero-group velocity of the helicon at that point.[16] The absorption edge at $\Gamma\approx1.02$ is understood by noting that

$$e^{-\alpha z}\cos(q_rz)\propto\int_0^\infty\frac{\alpha}{\alpha^2+(q-q_r)^2}\cos qz\,dq.$$

The spatially damped wave includes, therefore, $q$ values in the range $q\approx q_r-\alpha$ to $q\approx q_r+\alpha$. At $\Gamma=1$, $\alpha/q_r=4\times10^{-2}$ [see Fig. 1(c)] and rapidly drops as $\Gamma$ exceeds unity, yielding an absorption edge at 1.02. Alternatively, one may calculate the energy gained by an electron whose transverse velocity component is initially parallel to the electric field as

$$e\int_0^\infty\mathbf{E}\cdot d\mathbf{l}\propto\int_0^\infty e^{-\alpha z}\cos\left[\left(\frac{\omega_c^*}{v_z}-q_r\right)z\right]dz$$
$$\propto\frac{1}{\alpha}\left(1+\frac{(\omega_c^*/q_rv-1)^2}{\delta^2}\right),$$

where $\delta=\alpha/q_r$. Thus, at $\Gamma=1$ absorption takes place by electrons having $v>v_z>v(1-\delta)$.

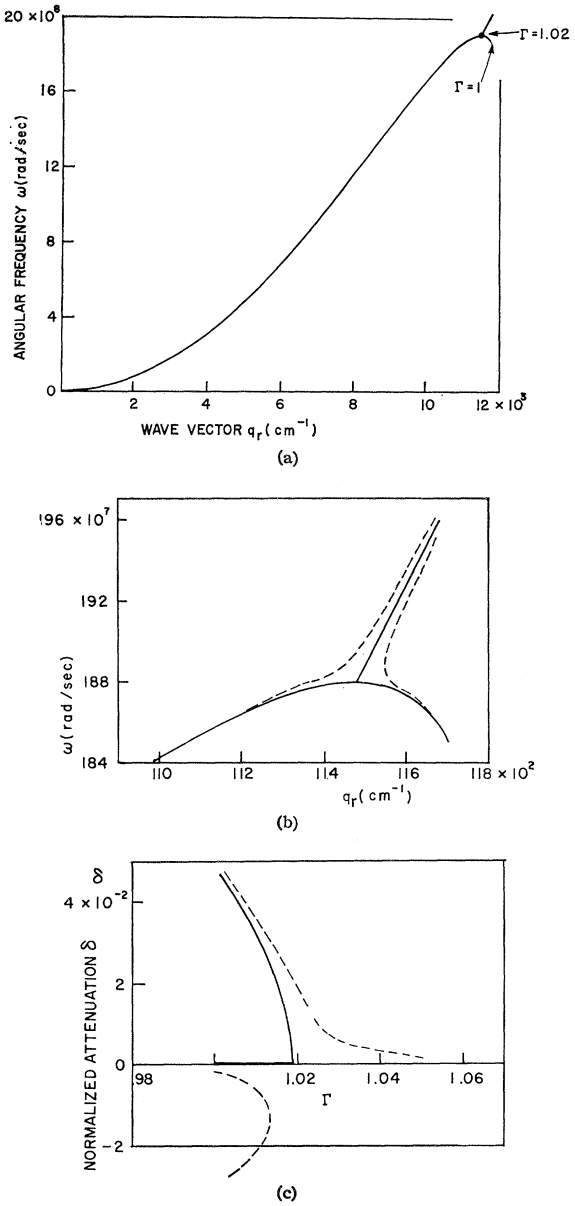


FIG. 1. Computed helicon dispersion and attenuation in potassium for a magnetic field of 57.9 kG. (a) Over-all dispersion curve in the collisionless limit; (b), (c) details of dispersion and normalized attenuation $\delta=\alpha/q_r$ in the absorption-edge region, solid curves: collisionless limit, dashed curves: $\tau=10^{-9}$ sec.

[15] A. W. Overhauser and S. Rodriguez, Phys. Rev. **141**, 431 (1966).

[16] J. C. McGroddy, J. L. Stanford, and E. A. Stern, Phys. Rev. **141**, 437 (1966).

A magnified view of the dispersion in the edge region and a normalized attenuation plot are given respectively in Figs. 1(b) and 1(c). Clearly, the absorption has reached an appreciable value at $\Gamma=1$. The dashed curves in these figures show the results of computations made with $\tau=10^{-9}$ (for which $\omega_c^*\tau=1180$, assuming $\beta=1.16$).[17] Collisions blur the edge and disconnect the branches. The negative attenuation coefficient of the right-hand branch, as well as the negative slope of its dispersion curve in the small damping region, suggests a backward wave. The exact physical interpretation of this backward-wave branch is not completely clear. It may be difficult to detect because of the narrow frequency range over which damping is not overwhelming.

## V. HELICON-ACOUSTIC INTERACTION: ANALYTIC TREATMENT

Helicon and acoustic waves interact via the electron currents that accompany each of these wave types. As a consequence of this interaction, a set of two new eigenmodes, neither of which can be identified as purely helicon nor acoustic, replace the latter as the independent propagating waves of the system. The dispersion relations of these eigenmodes are given by the solutions of the complete secular equation (13). As discussed in Sec. IV, with $\omega_c^*>0$, the propagating helicon is the + mode. Equation (13) indicates that it is coupled only to the + polarized acoustic wave. For convenience, we rewrite this equation in the form

$$(q^2-Q_h^2)(q^2-Q_p^2)-Q_i^2q^2=0, \tag{32a}$$

where

$$Q_h^2(q,\omega)=i\beta(\omega_p/c)^2\omega\tau G^+, \tag{32b}$$

$$Q_p^2(q,\omega)=\frac{\omega^2}{c_s^2}+\rho\frac{\beta\omega_c^*\omega}{c_s^2}-i\frac{\rho\beta\omega}{c_s^2\tau}\left(1-\frac{1}{G^+}\right), \tag{32c}$$

$$Q_i^2(q,\omega)=-\frac{\rho\omega}{c_s^2}\left[\omega_c^*\left(1-\frac{1}{\beta}\right)-\frac{i}{\tau}\left(1-\frac{1}{G^+}\right)\right]\times[\beta(1-G^+)+i\omega_c^*\tau(1-\beta)G^+]. \tag{32d}$$

The quantities $Q_h^2$ and $Q_p^2$ are, respectively, the squares of the wave vectors of the uncoupled helicon and acoustic waves. The coupling is represented by $Q_i^2$.

Although (32) is transcendental in $q$ except in the high-field limit, the relatively weak frequency dependence of the conductivity function permits it to be regarded as a cubic equation in $\omega$. Quinn and Rodriguez[6] found solutions of this cubic for the free-electron counterpart of (32). Their approach permitted study of temporal damping inside the DSCR edge, but is inconvenient for the treatment of spatial damping. In this section, we shall be content with wave-vector solutions of (32) that, while only approximate, serve to elucidate the dependence of the helicon-acoustic interaction on the relaxation time and effective mass.

Solving (32a) as a quadratic in $q$ yields

$$q^2=\tfrac{1}{2}(Q_h^2+Q_p^2+Q_i^2)\pm\tfrac{1}{2}[(Q_h^2-Q_p^2)^2+Q_i^2(2Q_h^2+2Q_p^2+Q_i^2)]^{1/2}. \tag{33}$$

Because the $Q$'s themselves are $q$-dependent, (33) only provides a general dispersion relation for each eigenmode rather than completely defined solutions for $q$. However, it is still possible to obtain a good amount of information from this equation without actually determining these dispersion relations. Let us, first, define the crossover frequency $\omega_x$ and crossover wave vector $q_x$. These quantities are taken to be the frequency and wave vector at which the helicon and acoustic dispersion relations would (possibly) intersect if the coupling term $Q_i^2$ were zero; i.e., with $Q_i^2=0$ and $\omega=\omega_x$ the solutions of (33) satisfy the relation $\mathrm{Re}(q)=q_x=\mathrm{Re}(Q_h)=\mathrm{Re}(Q_p)$. It is also worthwhile to review briefly the behavior of (33) with finite coupling for the lossless case in which $Q_h^2$, $Q_p^2$, and $Q_i^2$ are positive real. Sufficiently far from the crossover frequency $|Q_h^2-Q_p^2|\gg Q_i^2$, permitting the solutions of (33) to be represented by

$$q^2\approx Q_h^2[1+Q_i^2/(Q_h^2-Q_p^2)], \tag{34a}$$

$$q^2\approx Q_p^2[1+Q_i^2/(Q_p^2-Q_h^2)]. \tag{34b}$$

Equations (34a) and (34b) display the tendency of the eigenmode wave vectors to be increasingly pushed apart by the interaction as $\omega_x$ is approached. The main feature of the interaction at $\omega=\omega_x$ is retained if one assumes that $Q_i\ll q_x$ and evaluates the right-hand side of (33) for $q=q_x$. This approximation reduces (33) to

$$q\approx q_x\pm\tfrac{1}{2}Q_i, \tag{35}$$

and shows that the degeneracy of the eigenmodes at the crossover is broken in first order in $Q_i$. The mode splitting $\Delta q$, which is defined as the difference between the eigenmode wave vectors at the crossover, is itself seen to be approximately equal to $Q_i$. In the crossover region neither mode is predominantly acoustic nor heliconlike in character. We shall use the term "P mode" to refer to the eigenmode which starts out phononlike at low frequencies and becomes heliconlike above the crossover frequency. The mode which is heliconlike at low frequencies will be called the H mode. Typical P- and H-mode dispersion curves are sketched in Fig. 2. The behavior of the mode splitting and the attenuation of the eigenmodes for several regimes of interest are treated below.

### A. High-Field Limit: $(qv/\omega_c^*)\to 0$, $\omega_c^*\tau\gg 1$

This is the local conductivity regime considered in Sec. IV A. Equation (26) for $G^+$ may be used in (32b)

[17] This effective-mass ratio is based on the calculation of J. Callaway, Phys. Rev. **119**, 1012 (1960).

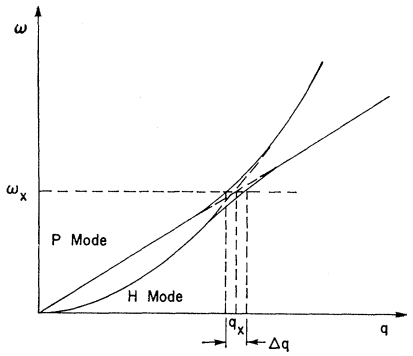


FIG. 2. Typical eigenmode dispersion resulting from the helicon-acoustic interaction. The dashed curves represent the uncoupled helicon and acoustic modes.

and (32d), yielding

$$Q_h^2 \approx \beta \frac{\omega}{\omega_c^*}\left(\frac{\omega_p}{c}\right)^2\left(1-\frac{1}{i\omega_c^*\tau}\right)=\frac{4\pi ne}{B_0 c}\omega\left(1-\frac{1}{i\omega_c^*\tau}\right), \quad (36)$$

$$Q_i^2 \approx \rho\frac{\omega\omega_c^*}{\beta c_s^2}\left(1-\frac{1}{i\omega_c^*\tau}\right)=\frac{eB_0}{Mcc_s^2}\omega\left(1-\frac{1}{i\omega_c^*\tau}\right). \quad (37)$$

In order to avoid introduction of a spurious imaginary term into $Q_p^2$, it is necessary to employ the more accurate local conductivity function

$$G^+=1/[1+i(\omega_c^*-\omega)\tau] \quad (38)$$

in (32c). That equation then becomes

$$Q_p^2=\omega^2/c_s^2+\rho\beta\omega^2/c_s^2\approx\omega^2/c_s^2, \quad (39)$$

where in the second form of writing, we have dropped only an insignificant constant renormalization of the sound velocity. Inspection of (36), (37), and (39) discloses that these quantities do not involve the free-electron mass, while the effective mass enters only through the dissipative factor $1/i\omega_c^*\tau$. To the extent that it is not affected by collisions, we can, thus, expect the mode splitting to be independent of the mass. The attenuation of the eigenmodes will necessarily be proportional to $m^*$. Speculations that have been made[4] with respect to the possible presence of a factor $(1-m/m^*)$ appear to be unfounded.

To determine the crossover frequency, one equates (39) to the real part of (37). This yields

$$\omega_x=4\pi nec_s^2/B_0c. \quad (40)$$

It follows that the crossover wave vector $q_x$ is given by

$$q_x=4\pi nec_s/B_0c. \quad (41)$$

We may approximate the mode splitting by $\mathrm{Re}(Q_i)$, using the crossover frequency given by (40) in (37). The result can be written in the form

$$\Delta q\approx\Omega_p/c, \quad (42)$$

where $\Omega_p=(4\pi ne^2/M)^{1/2}$ is the ion-plasma frequency. Hence, in this regime the splitting is independent of both the magnetic field and sound velocity, while the relative mode splitting $\Delta q/q_x$ increases with decreasing crossover frequency and wave vector. The approximation $\Delta q\approx\mathrm{Re}(Q_i)$, therefore, becomes inaccurate when the magnetic field is so high that $q_x$ is no longer larger than $\mathrm{Re}(q_i)$. For potassium, with a fast sound-wave velocity of $1.69\times10^5$ cm/sec, a magnetic field strength of 100 kG leads to $\omega_x=8.15\times10^8$, $q_x=4.82\times10^3$ cm$^{-1}$, and $\Delta q\approx0.84\times10^3$ cm$^{-1}$. The relative mode splitting is, thus, about 17%. At the crossover $\Gamma_0=4.25$, showing that the conductivity, which was assumed to be local, is actually moderately nonlocal.

To find the attenuation of the eigenmodes at the crossover frequency for the case $q_x\gg\mathrm{Re}(Q_i)$, $1/\omega_c^*\tau\ll\mathrm{Re}(Q_i)/q_x$, it is sufficient to approximate (33) by

$$q^2\approx q_x^2(1-1/2i\omega_c^*\tau)+\tfrac{1}{2}\,\mathrm{Re}(Q_i^2)\pm q_x\,\mathrm{Re}(Q_i)(1-3/4i\omega_c^*\tau). \quad (43)$$

One then obtains

$$\alpha_{\substack{\mathrm{H}\\\mathrm{P}}}\approx\frac{q_x}{4\omega_c^*\tau}[1\pm\tfrac{3}{2}\,\mathrm{Re}(Q_i)/q_x]. \quad (44)$$

Division of $\alpha_H$ and $\alpha_P$ by $q_H$ and $q_P$, respectively, yields the normalized eigenmode attenuations

$$\delta_{\substack{\mathrm{H}\\\mathrm{P}}}\approx(4\omega_c^*\tau)^{-1}[1\pm\mathrm{Re}(Q_i)/q_x]. \quad (45)$$

Equations (44) and (45) indicate that the attenuation of each eigenmode is close to half that of the uncoupled helicon, as given by (29); i.e., at the crossover frequency, the dissipation of the pure helicon is shared almost equally between the two. The lack of complete equality, which is proportional to the mode splitting, is due to the collision-dependent part of the coupling term. It can be shown[7] to arise, primarily, as a consequence of the collision drag force, which as a *coherent* collision-dependent force, is not necessarily dissipative in its total effect. It is, therefore, capable, of decreasing the attention of one eigenmode, while it increases that of the other.

Sufficiently strong damping can also reduce the mode splitting. The effect of the coupling is diminished because the complex wave vector of the damped helicon cannot match the real wave vector of the dissipationless sound wave. At the crossover, (33) may be put into the form

$$q^2=q_x^2\left\{\left[1-1/2i\omega_c^*\tau+\frac{1}{2}\frac{\mathrm{Re}(Q_i^2)}{q_x^2}(1-1/i\omega_c^*\tau)\right]\pm\frac{1}{2}\left[\frac{\mathrm{Re}(Q_i^2)}{q_x^2}(1-1/i\omega_c^*\tau)[4q_x^2+\mathrm{Re}(Q_i^2)-(2q_x^2+\mathrm{Re}(Q_i^2))/i\omega_c^*\tau]-1(\omega_c^*\tau)^2\right]^{1/2}\right\}. \quad (46)$$

We previously made the assumption $1/\omega_c{}^*\tau \ll \mathrm{Re}(Q_i)/q_x$ and were thus able to neglect the subtractive last term in the square root in (46). It is clear, however, that as $1/\omega_c{}^*\tau$ approaches $2\,\mathrm{Re}(Q_i)/q_x$ in magnitude, the real part of the square root must decrease rapidly, causing a similarly rapid drop in the mode splitting. On the other hand, the imaginary part of the square root increases, resulting in an enhancement of the attenuation of one eigenmode and a diminution in that of the other. When $1/\omega_c{}^*\tau$ exceeds $2\,\mathrm{Re}(Q_i)/q_x$, the real part of the argument goes negative and the square root becomes predominantly imaginary. By this time, the mode splitting is greatly diminished, although the disparity between the attenuations is only now at the point of beginning its biggest increase. Finally, for $1/\omega_c{}^*\tau \gg 2\,\mathrm{Re}(Q_i)/q_x$, (46) reduces to the set of approximate solutions $q^2=q_x{}^2(1+i/\omega_c{}^*\tau)$, $q^2=q_x{}^2$, which may be identified, respectively, with the wave vectors of the heavily damped pure helicon and the undamped acoustic wave at the crossover, i.e., the helicon-acoustic interaction is effectively nullified by the strong dissipation of the helicon. We have made numerical calculations, which indicate similar behavior when the crossover occurs at wave-vector values for which the conductivity is nonlocal.

### B. Collisionless Limit with Moderately High Field: $\omega_c{}^*\tau \to \infty$, $(qv/\omega_c{}^*) \ll 1$

Under these conditions (identical to Sec. IV B), both the helicon and acoustic waves are lossless and the conductivity is moderately nonlocal. Using (30) for $G^+$, (32b)–(32d) become

$$Q_h{}^2 \approx \beta \frac{\omega}{\omega_c{}^*}\left(\frac{\omega_p}{c}\right)^2\left(1+\frac{1}{5\Gamma_0{}^2}\right)=\frac{4\pi ne}{B_0 c}\omega\left(1+\frac{1}{5\Gamma_0{}^2}\right), \tag{47a}$$

$$Q_p{}^2 \approx \frac{\omega^2}{c_s{}^2}+\frac{1}{5}\frac{\rho\beta}{c_s{}^2}\frac{\omega\omega_c{}^*}{\Gamma_0{}^2} \approx \frac{\omega^2}{c_s{}^2}, \tag{47b}$$

$$Q_t{}^2 \approx \frac{\rho\omega\omega_c{}^*}{\beta c_s{}^2}\left(1+\frac{1-2\beta}{5\Gamma_0{}^2}\right)=\frac{eB_0}{Mcc_s{}^2}\omega\left(1+\frac{1-2\beta}{5\Gamma_0{}^2}\right). \tag{47c}$$

Equation (47b) displays a sound-velocity variation proportional to the magnetic field and, in conformity with the treatment in Sec. III, inversely proportional to the square of the effective mass. In the present context, this variation may be ignored and has, therefore, been dropped in the second form of writing. There is also a nonlocal conductivity contribution to (47c), which results in a nonelementary dependence of $Q_t{}^2$, and hence, the mode splitting, on the effective mass. This represents a strain-dependent effect that can only arise when the Bloch electrons at the Fermi surface are capable of having their trajectories altered by the strain inhomogeneities associated with the wave. In a more complete theory, $Q_t{}^2$ would, therefore, also depend on the parameter $\gamma$ that we are ignoring here.

The main consequence of the nonlocal conductivity in this regime is a shift in the crossover to higher frequencies and wave vectors than would otherwise obtain. Equating (47a) to (47b) yields a quadratic relation in $q$, the roots of which are

$$q=\frac{5eB_0{}^3}{8\pi ncc_s{}^2(hk_F)^2}\left\{1\pm\left[1-\frac{4}{5}\left(\frac{4\pi nc_s hk_F}{B_0{}^2}\right)^2\right]^{1/2}\right\}. \tag{48}$$

The root of interest is the one closest to the crossover wave vector in the limit $k_F=0$, and is given by the minus sign in (48). It can be approximated by

$$q_x \approx \frac{4\pi ne}{B_0}\left(\frac{c_s}{c}\right)\left[1+\frac{1}{5}\left(\frac{4\pi nc_s hk_F}{B_0{}^2}\right)^2\right]. \tag{49}$$

The other root of (48), which is much larger, is in general without physical meaning; except under the most propitious circumstances it corresponds to a value of $q$ for which the approximation (30) for $G^+$ is not valid. The existence of a second crossover is, however, quite possible[5] and is treated in Sec. VI.

The approximate mode splitting is readily determined from the relation $\Delta q \approx Q_t$. Upon setting $\omega_x=c_s q_x$ in (47c) and taking the square root, one obtains

$$\Delta q \approx (eB_0 q_x/Mcc_s)^{1/2}[1+\tfrac{1}{10}(1-2\beta)(\hbar ck_F q_x/eB_0)^2]. \tag{50}$$

Equation (50) indicates that the nonlocality of the conductivity reduces the mode splitting. The actual amount of this reduction is dependent on $m^*$, the diminution being greatest for electrons of small effective mass. The numerical solutions in Sec. VI display a similar effective-mass dependence for an even more nonlocal conductivity. The effect, however, still remains quite small.

## VI. NUMERICAL COMPUTATIONS

This section presents the results of computations we have made for the helicon-acoustic interaction in potassium. An IBM 7040 computer was used to obtain numerical solutions of the full secular equation (13), wherein the conductivity function was represented exactly by (6). The wave vectors and attenuation coefficients were determined for frequencies and magnetic fields chosen such that crossover occurred under conditions of nonlocal conductivity.

Figure 3 is a plot of the independent dispersion curves for the fast acoustic wave and uncoupled helicon waves, in the lossless limit, for $B_0=59.9$, 58.9, and 57.9 kG; the damped branches of the helicon-dispersion relations are not shown. Extreme sensitivity of the crossover to small variations in field strength is evident, a 4% decrease in $B_0$ being sufficient to go from a crossover at $\Gamma \approx 1.3$ to an absence of crossover with the lossless branch of the helicon. (There can still be a crossover with the damped branch.) The 58.9-kG helicon dis-

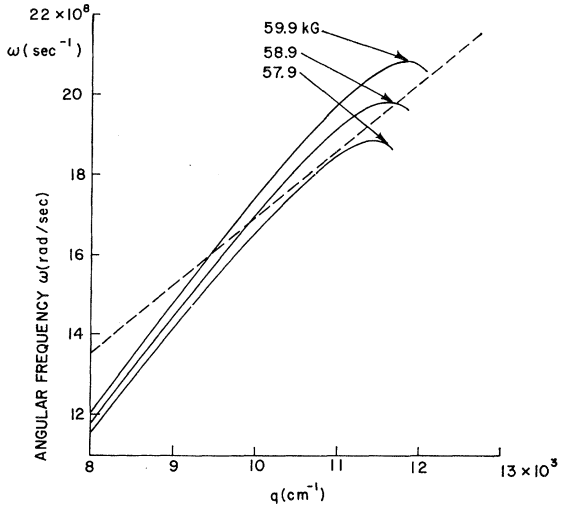


FIG. 3. Dispersion curves for fast acoustic wave (dashed line) and helicon wave (solid curves) in potassium for three values of magnetic field.

plays a double crossover, made possible by the bend-over of the curve. Quinn and Rodriguez[6] have pointed out that a third crossover can take place in the temporally damped region beyond the DSCR edge. It may be inferred from the figure that the spatially damped branch can also provide a third crossover point.

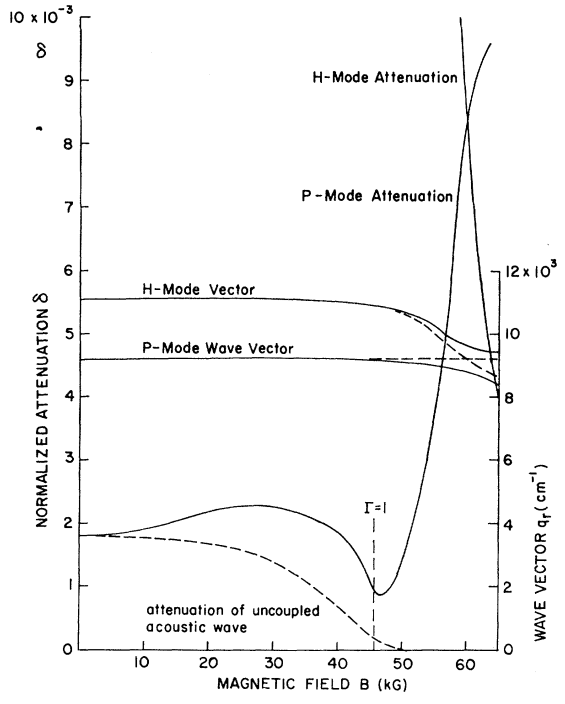


FIG. 4. Computed wave vectors and normalized attenuation of eigenmodes in potassium for variable magnetic field $\omega=1.55\times10^9$ rad/sec, $\tau=4\times10^{-11}$ sec, $\beta=1.16$. The dashed curves denote the uncoupled helicon and acoustic wave vectors and the attenuation of the uncoupled acoustic wave.

Figure 4 is a composite of curves showing the gross features of the helicon-acoustic interaction with the frequency fixed at $\omega=1.55\times10^9$ and the magnetic field swept from zero to 65 kG. A value of $\tau=4\times10^{-11}$, attainable in potassium of reasonable purity at helium temperatures, was selected for these computations. The parameter $\Gamma=1.34$ at the crossover, indicating that the conductivity is strongly nonlocal in the interaction region. At the right-hand side of the figure, with $B_0=65$ kG, the crossover frequency lies below $1.55\times10^9$, and according to the convention adopted earlier, the H mode is phononlike, the P mode heliconlike. Proceeding to the left, through the interaction region, their roles become interchanged. Correspondingly, the attenuation of the P mode drops, while that of the H mode goes beyond the scale of the figure. At still smaller fields the wave vectors of both modes lose their magnetic field dependence, the P mode most rapidly. Because of the finite relaxation time, the H mode makes a smooth transition to the spatially damped upper branch [see Fig. 1(b)], and although it is already off-scale in Fig. 4, its attenuation rises steadily. Because the parameters chosen here correspond to an electronic mean free path much greater than a classical skin depth, it becomes an anomalous skin-effect excitation,[18] as zero field is approached. At the magnetoacoustic absorption edge, $\Gamma=1$, the P mode is substantially phononlike, and its wave vector is therefore nearly field-independent. However, comparison of its attenuation with that of the uncoupled acoustic wave (shown by the dashed curve) indicates that there is still enough residual dissipation resulting from interaction with the highly damped helicon to spoil the appearance of the edge.

Inside the edge, a hump in the P-mode attenuation curve further distinguishes its absorption characteristics from that of the pure acoustic wave. The H-mode wave vector does not depart from the P-mode wave vector by more than 20% for the entire low-field portion of the field sweep. It is thus possible for it to "share" some of its rapidly increasing dissipation with the P mode and thereby increases the attenuation of the latter, although the effect of the interaction no longer shows up in the real part of the P-mode wave vector. As zero field is approached, the H-mode dissipation finally becomes so large that interaction is prevented and the P-mode attenuation reverts to that of the independent acoustic wave. This behavior is in agreement with the treatment given in Sec. V, although that was restricted to the effect of strong collisional damping on the eigenmodes at the crossover.

In the limit of large discrepancy between the P-mode and H-mode wave vectors the frequency dependence of the hump is easily determined. We start from (34b), which remains valid in the dissipative case. Taking the

[18] A. B. Pippard, G. E. H. Reuter, and E. H. Sondheimer, Phys. Rev. 73, 920 (1948).

square root and introducing the assumption $|Q_h|\gg|Q_p|$ reduces that relation to

$$q_P\approx Q_p[1-Q_i^2/2Q_h^2]. \tag{51}$$

Hence,

$$\alpha_P\approx \mathrm{Im}[Q_p(1-Q_i^2/2Q_h^2)]. \tag{52}$$

The essential physics is retained in the collisionless limit and free-electron model. Therefore, we let $\beta=1$ and $\tau\to\infty$, for which (32d) becomes

$$Q_i^2=-i\rho\omega/c_s^2\tau G^+. \tag{53}$$

Inserting (53), (32b), and (32a) into (52), and using the inequality $\mathrm{Im}(Q_p)\ll\mathrm{Re}(Q_p)$, yields

$$\alpha_P\approx\left[1+2\frac{\omega}{\omega_p^2}\left(\frac{c}{c_s}\right)^2\mathrm{Im}\frac{1}{\tau G^+}\right]\left[\frac{\rho}{2c_s}\mathrm{Re}\frac{1}{\tau G^+}\right]. \tag{54}$$

Comparison of this equation with (17) reveals that the factor in the second pair of brackets is the expression for the magnetoacoustic attenuation in the collisionless case when there is quasibalance of currents. Accordingly, we rewrite (54) as

$$\alpha_P\approx\left[1+2\frac{\omega}{\omega_p^2}\left(\frac{c}{c_s}\right)^2\mathrm{Im}\frac{1}{\tau G^+}\right]\alpha_0, \tag{55}$$

where $\alpha_0$ designates the current-balance magnetoacoustic attenuation. Outside the absorption edge, $\alpha_0=0$. Just inside the edge, $G^+$ within the bracket in (55) may be approximated by its edge value (51). This results in

$$\alpha_P\approx\left[1+\frac{4}{3}\left(\frac{c}{c_s}\right)^2\frac{\omega\omega_c}{\omega_p^2}\right]\alpha_0, \tag{56}$$

and upon employing $\omega=qc_s=\omega_c c_s/v$,

$$\alpha_P\approx\left[1+\frac{4}{3}\frac{c^2\omega_c^2}{vc_s\omega_p^2}\right]\alpha_0=\left[1+\frac{\pi B_{\mathrm{edge}}^2}{\hbar c_s k_F^4}\right]\alpha_0. \tag{57}$$

Thus, interaction with the H mode brings about a relative increase of approximately $\pi B_{\mathrm{edge}}^2/\hbar c_s k_F^4$ in the attenuation near the edge. On the other hand, one may show from (19) that the zero-field limit of $\tau G^+$ is $3\pi/4qv$; its imaginary part is very small. Therefore, after an initial overshoot producing a hump or peak, $\alpha_P$ eventually comes back into coincidence with the $\alpha_0$ at zero field. This discrepancy between the $\alpha_P$ and $\alpha_0$ curves may also be viewed simply as a consequence of current balance breakdown due to the magnetic field, rather than as a result of helicon-acoustic interaction. In the absence of the field such breakdown can only occur at very high frequencies, well in excess of $10^9$ sec$^{-1}$, for which the zero-field limit of $\mathrm{Im}(\tau G^+)$ is no longer negligible.

Although (57) was derived with the restrictions $\tau\to\infty$ and $|Q_h|\gg|Q_p|$, for the value of the edge field in Fig. 4, it works out numerically to $\alpha_P=2.15\ \alpha_0$, in fair agreement with the ratio of the attenuations just inside the absorption edge in that figure. According to (57), the magnitude of the effect should be proportional to the square of the edge field, and hence the square of the edge frequency. It is expected to be much smaller in metals other than potassium because of the factor $c_s k_F^4$ in the denominator; therefore, large distortions of the acoustic absorption edge should be rather rare. Nevertheless, experimental verification of this breakdown of current balance at moderate frequencies would be desirable; the field strengths and sample purities required for its investigation in potassium are not unreasonable.

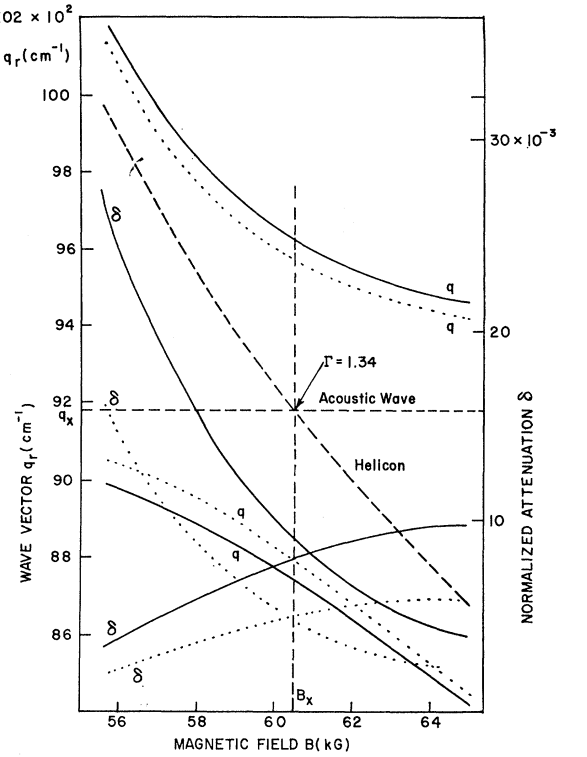


FIG. 5. Detailed behavior of eigenmode wave vectors and normalized attenuation in the crossover region $\omega=1.55\times10^9$ rad/sec, $\tau=4\times10^{-11}$ sec. The solid curves are for $\beta=1.16$, the dotted curves for $\beta=2$. The dashed curves denote the wave vectors of the uncoupled helicon and acoustic modes.

The detailed behavior of the eigenmodes in the strong interaction region, which occupies the extreme right-hand portion of Fig. 4, is displayed in Fig. 5. In this figure the frequency and relaxation time are unchanged, but the field is swept only over the limited range 55.7 to 65 kG. The dotted curves represent the results of calculations made for a hypothetical effective-mass ratio $\beta=2$, and are included to show the sensitivity of the attenuation and mode splitting to the effective mass. The relative mode splitting is 9.7% for $\beta=1.16$ and 8.5% for $\beta=2$. This change appears quite small in view of the great variation in effective mass. However,

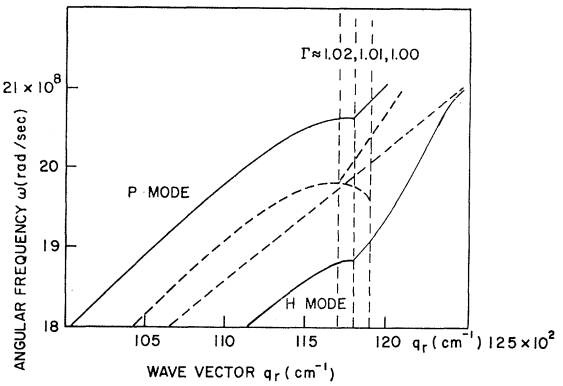


FIG. 6. Eigenmode dispersion curves for crossover in the absorption-edge region in potassium in the collisionless limit. $B_0=58.9$ kG, $\beta=1.16$. The dashed curves represent the uncoupled modes.

it is slightly larger than is predicted by (50), a formula meant to be applicable when the conductivity is only weakly nonlocal. The mode splitting difference would be accentuated by the absence of dissipation. With $\tau=4\times10^{-11}$, the values of $\omega_c{}^*\tau$ at the crossover field are 49 for $\beta=1.16$ and 85 for $\beta=2$. The higher attenuation of the $\beta=1.16$ eigenmodes due to the smaller cyclotron frequency is a significant feature of Fig. 5. According to the analysis in Sec. V, this should result in a diminution of the mode splitting, a tendency in opposition to the nonlocal effect of variations in $\beta$.

Crossover in the edge region is considered in Fig. 6, which displays the computed eigenmode dispersion curves for interaction between the acoustic wave and 58.9-kG helicon. This is the double-crossover situation depicted in Fig. 3. The uncoupled modes are shown again in Fig. 6 by the dashed curves, this time with the upper branch of the helicon included. The plot is for $\beta=1.16$ and an infinite relaxation time, chosen to sharpen the details of the interaction. We have swept the frequency from $\omega=1.8\times10^9$ to $2.1\times10^9$. Figure 6, therefore, covers only the more interesting region in the vicinity of the upper crossover and the absorption edge. Because of the lower crossover the P mode appears to the left, the H mode to the right. Starting from $\omega=1.8\times10^9$, there is a broad interaction region in which the mode splitting is about 10% and the eigenmode dispersion curves are substantially straight and parallel. This region, in which the group velocities remain nearly equal, extends down to the vicinity of the lower crossover. Slightly above $\omega=1.88\times10^9$, there is a sudden break in the H-mode curve, and it begins to run parallel to the upper branch of the helicon, showing no evidence of interaction with the backward wave branch. This is the absorption edge for the H mode and corresponds to $\Gamma\approx1.01$. It thus lies inside the absorption edge of the pure helicon at $\Gamma=1.02$ and outside the magnetoacoustic edge at $\Gamma=1$. Going to higher frequencies, the H-mode wave vector eventually becomes asymptotic to that of the uncoupled acoustic wave. As it does so, its attenuation (not displayed) begins to drop since the attenuation of the latter, even inside the edge, is quite small compared with that of the helicon. The P mode roughly follows the shape of the pure helicon, becoming asymptotic to the upper branch. Here, too, attenuation begins at $\Gamma\approx1.01$, but then rises more steeply than that of the H mode. The frequency range between the two break points is one of some interest, since within it only one of the eigenmodes is dissipative. Although the break points and absorption edges will be blurred in the presence of collisions, for large $\omega_c{}^*\tau$ the general features of the interaction should remain intact.